Acta Astronautica 138 (2017) 225–232

Contents lists available at ScienceDirect

Acta Astronautica

journal homepage: www.elsevier.com/locate/actaastro

Hayabusa 2 extension plan: Asteroid selection and trajectory design

Bruno Victorino Sarli *, Yuichi Tsuda

Department of Space Flight Systems, Japan Aerospace Exploration Agency, 3-1-1 Yoshinodai, Chuo, Sagamihara, 252-0222, Japan

ARTICLE INFO

Keywords:
Low-thrust trajectory design
Asteroid selection
Hayabusa 2
Asteroid flyby

ABSTRACT

The Hayabusa 2 mission is targeted to explore the asteroid (162173) 1999 JU_3 and return surface as well as subsurface samples through a novel impactor. Upon its return, at the end of 2020, the spacecraft will release the capsule for Earth re-entry and drift away from the planet. Based on the current mission profile, the spacecraft is expected to retain 30 kg of xenon propellant for trajectory maneuvers after the capsule is released. This remaining fuel can be used to extend the mission and improve its scientific return by exploring a new target. Work herein outlines an extension plan for Hayabusa 2, detailing the target selection process and its subsequent trajectory design. Due to final Earth escape trajectory, considering the excess velocity and orbital geometry, the only available extension option is an asteroid flyby. One of the most important trajectory characteristic is to maximize the spacecraft's optical detection capabilities. As a result the asteroid 2001 WR_1 is identified as the most promising target candidate. The resulting trajectory uses all the available xenon with 100% duty cycle. Furthermore, the extension lasts for 932 days and offers 1.57 days of optical navigation time for a flyby on June 27, 2023.

1. Introduction

After the success of Hayabusa [1], JAXA planned and launched its second asteroid sample return mission, Hayabusa 2, on 3 of December 2014 [2]. The mission targets the C-type asteroid (162173) 1999 JU_3, also known as Ryugu, to study the origin and evolution of the solar system as well as the building block materials for life. Hayabusa 2 mission was launched in a near 1:1 resonant orbit with Earth, which allowed it to perform a gravity assist one year later changing the spacecraft orbital inclination. The spacecraft uses μ 20 ion engines to maneuver in deep space and rendezvous with the asteroid (162173) 1999 JU_3 [3]. After an exploration campaign at the asteroid that will last roughly 18 months, the mission returns to Earth and releases a capsule containing surface and subsurface material collected from Ryugu for further analysis. Both surface collection methods involve novel techniques for the robotic arm. In particular, the subsurface collection method employs a plastic-based impactor to clear the surface area and give access to subsurface material. This study presents one of the mission's extension scenarios which begins after the capsule release and as the spacecraft returns to deep space. Several hours prior to the atmospheric entry, the spacecraft releases the capsule and performs chemical burns that define its new trajectory after the final Earth encounter. The mission is expected to remain with roughly 30 kg of xenon that can be used to steer the spacecraft to a new target.

One of the most important characteristics of the extension trajectory is the optical navigation time that the spacecraft has prior to the target encounter. The Hayabusa 2 spacecraft has a high definition camera used for close proximity operations on (162173) 1999 JU_3. This camera is capable of detailed imaging with a small observation angle and, due to this, the camera does not perform well for distance targeting. Its field of view is narrow, and it cannot identify distant objects - apparent visual magnitude detectable by the spacecraft camera is low. In the case of rendezvous with Ryugu, the arrival velocity is low and trajectory correction maneuvers near the encounter can be easily made. During the target arrival on the extension phase, however, the high definition camera has to be used for the encounter operations. Because of its poor performance for distant targets, sufficient time needs to be allocated for target identification and trajectory correction maneuvers. Therefore, in order to maximize the trajectory arrival robustness and the overall mission reliability, the objective for the trajectory design is to maximize the optical navigation time upon target arrival.

This work uses a combination of linear dynamics, optimal control as well as reachability theory to find potential targets and design a flyby trajectory [4] taking into account the full asteroid database [5]. The method for asteroid selection is based on a step process that progressively eliminates targets that are impossible to reach. It also provides a good estimation of the trajectory states and thrust profile for the final nonlinear optimization. Once the initial selection is made, asteroid and

* Corresponding author.
E-mail addresses: sarli@ac.jaxa.jp (B.V. Sarli), tsuda.yuichi@jaxa.jp (Y. Tsuda).

http://dx.doi.org/10.1016/j.actaastro.2017.05.016
Received 9 January 2017; Received in revised form 17 May 2017; Accepted 20 May 2017
Available online 23 May 2017

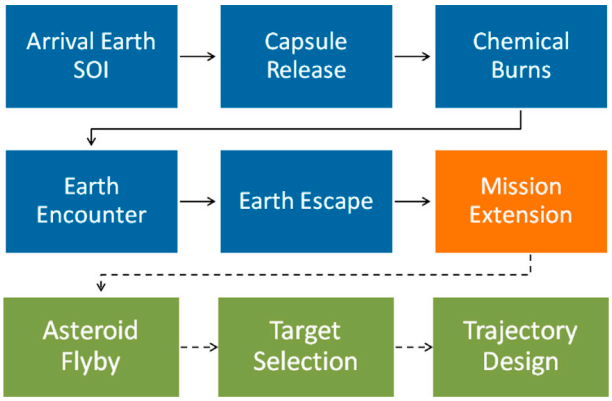

Fig. 1. Mission extension roadmap.

orbit characteristics - such as final mass, Sun-asteroid-spacecraft solar phase angle (SPV), H magnitude, asteroid spectrum type, time of flight and optical navigation time - are taken into account to further narrow the selection [6]. Finally, a global non-linear direct method optimization tool coupled with monotonic basing hopping [7,8] is used to calculate a trajectory with the maximum optical navigation time in the target arrival. A set of possible targets and their associated trajectories are defined through this method for the Hayabusa 2 extension mission. A final application of these results will depend on a successful Earth return and a proper execution of the pre-entry maneuvers.

After this introduction, the paper provides a general overview of the Hayabusa 2 mission in section 2. The details of the mission extension analysis as well as mission component segmentation are described in section 3. In section 4, the spacecraft dynamics and equations for calculating the optical navigation time are detailed. Sections 5 and 6 outline the theories and results achieved in the target selection and trajectory design, respectively. Finally, section 7 presents the conclusions of this work.

2. The Hayabusa 2 mission

Asteroid Explorer Hayabusa 2 is a successor of the previous Hayabusa mission, also known as MUSES-C. The first Hayabusa was successful in operating several new technologies and returning to Earth samples of the Apollo asteroid (25143) 1998 SF_{36}, also known as Itokawa [10], in June 2010. Together with establishing a new navigation method using solar electric propulsion for asteroid sample return, the mission was the first to bring to Earth asteroid samples that help to elucidate the origin of the solar system. Similar to its predecessor, Hayabusa 2 targets the exploration of the C-type asteroid (162173) 1999 JU_3, leveraging the experience acquired from the Hayabusa mission. C-type asteroids are primordial bodies expected to be rich in organic or hydrated minerals [9]. Basic elements forming the Earth's minerals and seawater as well as the building blocks of life are believed to have originated in the primitive solar nebula of the early solar system.

Hayabusa 2 builds on the electric propelled round-trip exploration technology developed by the Hayabusa mission, but also develops new technology to construct the basis for future deep space exploration. Spacecraft configuration is very similar to its predecessor. Key modifications include the flattened double antenna, previously single parabolic, and the new plastic-based impactor. The impactor creates an artificial crater that exposes subsurface material, which is less weathered by the space environment and heat. With this, both surface and sub-surface samples can be acquired in a single sample mission. Hayabusa 2 was launched on 3 of December, 2014 and is predicted to arrive at the C-type asteroid in mid 2018. Science on the asteroid will last 1.5 years with the spacecraft asteroid departure expected at the end of 2019 and Earth return in December 7, 2020 [11].

3. Mission extension design method

The extension mission starts once the spacecraft escapes from the Earth after the capsule is released, Fig. 1. Earth escape conditions are fixed based on the capsule release requirements, which is a priority at the Earth encounter. Entry conditions targeting is made through chemical burns hours before the atmospheric entry. The resulting ballistic trajectory after the escape can be seen in Fig. 2, which is propagated for 5 years.

Once the chemical maneuvers are finished, the spacecraft's maneuverability capacity is very limited by the amount of xenon remaining, roughly 30 kg. However, the remaining xenon can still be used by the electric propulsion system to change the trajectory enough to fly by a new target, improving the mission's science return. The mission extension options become limited: given the orbit geometry and propellant available, both rendezvous and planetary encounters are impossible. Only a flyby mission can be realized within the spacecraft and orbit capabilities. Furthermore, asteroids and comets are the only suitable body for this extension due to their abundance. Priority is given to find a reasonable flyby trajectory that can be achieved with the available xenon while maximizing optical navigation time. As mentioned previously, Hayabusa 2 has a high definition camera for proximity operations.

The design process is then divided into two parts: target selection and trajectory design. First, the target selection makes use of the full Minor

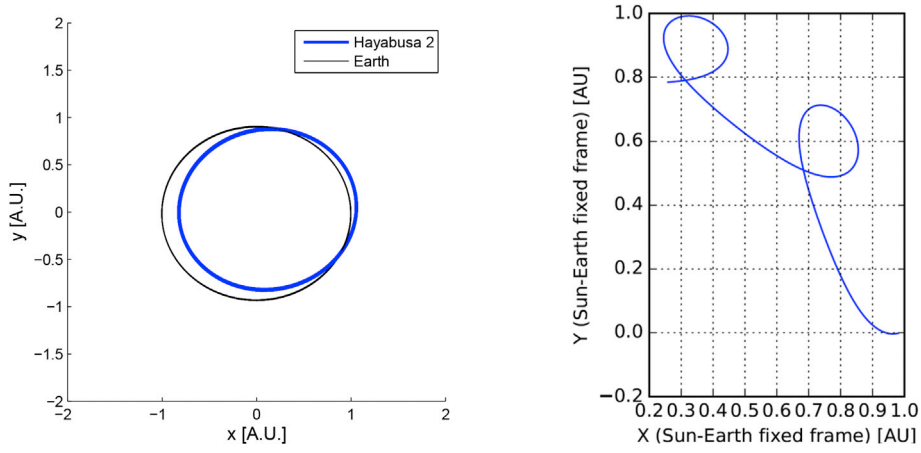

(a) Sun centered inertial frame (b) Sun-Earth rotating frame

Fig. 2. Hayabusa 2 final Earth escape trajectory.

Table 1
Hayabusa 2 spacecraft characteristics for the extended mission.

Min. dry mass	500 kg
Total mass	530 kg
Available Xe propellant	30 kg
Engine thrust	18e-3 N
Engine Isp	2800 s
Engine duty cycle	100%

Table 2
Constant values used in the calculation of the optical navigation time of the asteroid flyby.

Constant	V_{camera}	A_1	A_2	B_1	B_2
Values	8	3.33	1.87	0.63	1.22

Planet Center database (MPCORB) [5] together with a three step selection process to obtain candidate targets from the large database. Then, the trajectory design is made on selected candidates based on the estimated arrival conditions and physical characteristics of the target. With the selected candidates, the trajectory design objective, the cost function, becomes to maximize the spacecraft's optical navigation time at arrival while satisfying the spacecraft constraints. Table 1 presents the spacecraft characteristics that are of interest for this study.

4. Spacecraft and system modeling

Mathematical models that will be used throughout the paper are outlined in the next two subsections. First, the spacecraft model is derived considering a two-body model of a point mass with a fixed specific impulse (*Isp*) propulsion system. The second derivation deals with the available optical navigation time upon target arrival considering the spacecraft arrival conditions and the target physical characteristics.

4.1. Equations of motion

In this work, the equations related to trajectory design have three main forces acting upon it: Sun's gravity and the thrust generated by the propulsion system; Earth gravity is added as a perturbation. The dynamical system is described by 7 state variables, which are presented here in the inertial, Sun-centered, J2000 equatorial frame:

$$\mathrm{x} = [\mathbf{r}, \mathbf{v}, m]^t \tag{1}$$

$$\mathrm{p} = [\mathbf{u}, T]^t \tag{2}$$

$$\dot{\mathbf{x}} = f(\mathbf{x}, \mathbf{p}, t) = \begin{bmatrix} \dot{\mathbf{r}} \\ \dot{\mathbf{v}} \\ \dot{m} \end{bmatrix} = \begin{bmatrix} \mathbf{v} \\ -\mu \dfrac{\mathbf{r}}{r^3} + \mathbf{u}\dfrac{T}{m} \\ -\dfrac{T}{c} \end{bmatrix} \tag{3}$$

where $\mathbf{x}$ is a 7×1 state vector, $\mathbf{p}$ is a 4×1 control vector, $\mathbf{r}$ is a 3×1 position vector, $\mathbf{v}$ is a 3×1 velocity vector, m is the mass, $\mathbf{u}$ is a 3×1 unit vector that defines the thrust direction, μ is the central body gravitational parameter, T is the thrust magnitude and c is the propulsion exhaust velocity. The control variables are the thrust direction, $\mathbf{u}$, and throttled magnitude, T, which are constrained by the following relations:

$$\mathbf{u}^t\mathbf{u} = 1 \tag{4}$$

$$0 \leq T \leq T_{MAX} \tag{5}$$

Earth third body perturbations are considered for the non-linear optimization. In this case, the Earth's gravity acceleration is added to Eq. (3).

4.2. Optical navigation time

In the asteroid flyby portion of the extension mission, the optical navigation time is of great importance. It allows the identification of the target position to perform TCMs, navigation and science. Considering all the constraints, the trajectory would ideally have as much time as possible for optical navigation. The low-thrust trajectory design is then made such that the optical navigation time is the objective function [12].

The optical navigation time from an incoming spacecraft flying by an asteroid can be calculated as presented in Dymock, 2007 [13],

$$t_{obs} = \frac{10^{\beta}}{r_{ast}} \tag{6}$$

where t_{obs} is the observation time or optical navigation time in seconds and r_{ast} is the asteroid's position with respect to the Sun in normalized units (A.U. for this work),

$$\beta = \frac{V_{camera} - H_{\alpha}}{5} \tag{7}$$

$$H_{\alpha} = H_{ast} - 2.5\log_{10}[(1 - G_{ast})\phi_1 + G_{ast}\phi_2] \tag{8}$$

$$\phi_i = exp\left[- A_i \tan(\alpha/2)^{B_i}\right] \tag{9}$$

where, V_{camera} is the apparent visual magnitude detectable by the spacecraft camera, H_{ast} is the absolute visual magnitude of the asteroid, G_{ast} is the asteroid slope parameter (relates to the opposition effect - a surge in brightness, typically 0.3 magnitudes, observed when the object is near opposition [13]), A and B are constant properties of the camera, and α is the solar phase angle between the asteroid and the spacecraft (Sun-asteroid-spacecraft angle) which can be calculated as

$$\alpha = cos\left(\frac{\mathbf{r}_{ast}\cdot\mathbf{v}_{\infty}}{r_{ast}v_{\infty}}\right)^{-1} \tag{10}$$

where $\mathbf{v}_{\infty}$ is the spacecraft arrival velocity with respect to the asteroid. Table 2 shows empirical values for V_{camera}, A, and B used in this study.

Finally, the objective function for the optimization can be calculated as,

$$J = -t_{obs} \tag{11}$$

Therefore, J in Eq. (11), is the objective function to be minimized which means that, due to the negative sign, the optical navigation time is maximized.

5. Target selection

Using the ballistic Earth escape trajectory as reference, small changes in the spacecraft's orbit are possible using its electric propulsion system. As mentioned before, the amount of fuel available is modest, and the capability to change the orbit is going to be small. Based on this, suitable targets will lie close to the original orbit, close enough to consider them inside the orbit's linear region. Making use of this rationale and the MPCORB, a three step analysis is performed to identify target candidates for the non-linear trajectory optimization. This procedure is similar to what is done in Ref. [4] but with a change from a mid-course target to a final target, as done in Ref. [6].

5.1. Target selection steps

The first step in the target selection consists of obtaining the asteroid's position for the assumed maximum time of flight corresponding to the extended mission from the MPCORB. Here, the five years limiting time is based on an estimation of the maximum operation time allowed for the

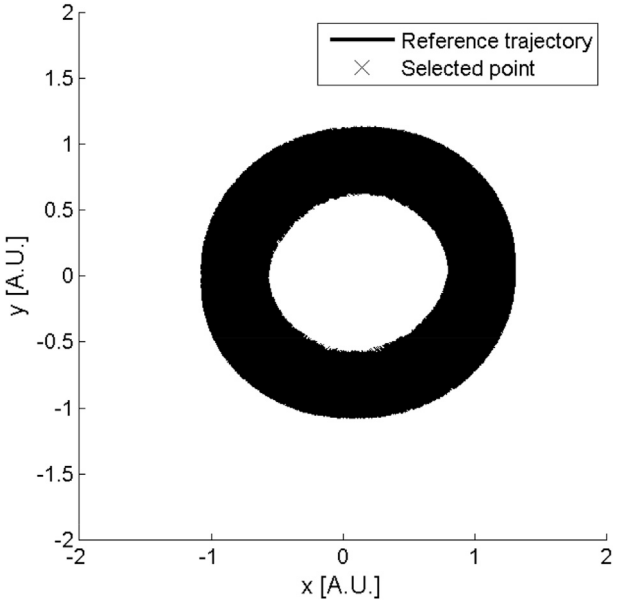

Fig. 3. First step selection.

spacecraft and some of the subsystems' life cycle. With the time of flight (ToF) defined, points on the asteroids' orbits that are further than 0.2 Astronomical Units (A.U.) from the reference orbit are considered unreachable and, therefore, are discarded. The selected maximum reachability of 0.2 A.U. is considered sufficient to encompass all possible solutions based on the capacity of the propulsion system. This first step decreases the possible number of flyby points, defined by a unique body combined with possible flyby epochs, by three orders of magnitude, as shown in Fig. 3.

The second step consists on the solution of a low-thrust linear Lambert approximation for each point of step 1. Linear low-thrust equations are derived based on the reference orbit, which is divided into segments that contain an impulse in its center. In this study, seven impulses were used. Being an intermediary selection step, the number of impulses will over-estimate the actual capacity of the low-thrust propulsion system, but will guarantee that no feasible points are lost. In this context, impulses can be calculated based on the state transition matrix,

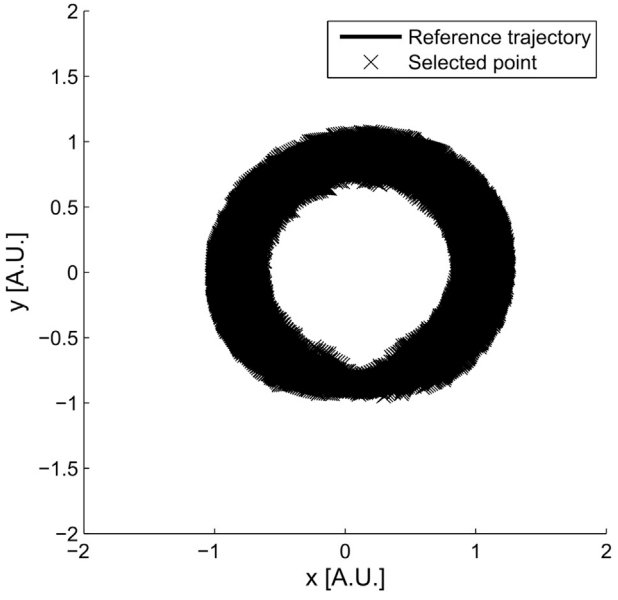

Fig. 4. Second step selection.

Φ, provided a deviation from the reference, $\delta = [\delta\mathbf{r}, \delta\mathbf{v}]$. Each point of the reference orbit is checked for every flyby point. The summation of the impulses, $\Delta\mathbf{v}$, can be calculated as

$$\begin{bmatrix}\delta\mathbf{r}\\ \delta\mathbf{v}\end{bmatrix} = \Phi(t_f, t_{n-1})\begin{bmatrix}\varnothing_{(3\times1)}\\ \Delta\mathbf{v}_{n-1}\end{bmatrix} + \Phi(t_f, t_{n-2})\begin{bmatrix}\varnothing_{(3\times1)}\\ \Delta\mathbf{v}_{n-2}\end{bmatrix} + \cdots + \Phi(t_f, t_0) \times \begin{bmatrix}\varnothing_{(3\times1)}\\ \Delta\mathbf{v}_0\end{bmatrix} \tag{12}$$

The δr is set to be the distance of the selected flyby point on step 1, and $\delta\mathbf{v}$ is ignored since this is a flyby. Therefore,

$$\delta\mathbf{r} = \Phi_R(t_f, t_{n-1})\begin{bmatrix}\varnothing_{(3\times1)}\\ \Delta\mathbf{v}_{n-1}\end{bmatrix} + \Phi_R(t_f, t_{n-2})\begin{bmatrix}\varnothing_{(3\times1)}\\ \Delta\mathbf{v}_{n-2}\end{bmatrix} + \cdots + \Phi_R(t_f, t_0) \times \begin{bmatrix}\varnothing_{(3\times1)}\\ \Delta\mathbf{v}_0\end{bmatrix} \tag{13}$$

where, Φ_R is the first three rows of the state transition matrix, $\Phi = \begin{bmatrix}\Phi_R\\ \Phi_V\end{bmatrix}$,

$$\delta\mathbf{r} = diag\left[\Phi_R(t_f, t_{n-1}), \cdots, \Phi_R(t_f, t_0)\right]\begin{bmatrix}\Delta\mathbf{v}_{n-1}\\ \Delta\mathbf{v}_{n-2}\\ \vdots\\ \Delta\mathbf{v}_0\end{bmatrix} \tag{14}$$

which can be re-written as,

$$\mathbf{a} = [\Phi_R]\Delta\mathbf{v} \rightarrow \mathbf{a} - \Phi_R\Delta\mathbf{v} = 0 \tag{15}$$

Given a cost function that minimizes the square of controls,

$$J = \frac{1}{2}\sum_{i=1}^{n-1}||\Delta\mathbf{v}_i||^2 \tag{16}$$

One can minimize this function by finding the extremals of the functional. Let $\overline{J}$ be the augmented functional given by J and its associated costates

$$\overline{J} = \frac{1}{2}\Delta\mathbf{v}^t\Delta\mathbf{v} + \lambda^t(a - \Phi_R\Delta\mathbf{v}) \tag{17}$$

with the extremals calculated by

$$\frac{\delta\overline{J}}{\delta\Delta v} = \Delta\mathbf{v}^t - \lambda^t\Phi_R = 0 \tag{18}$$

$$\Delta\mathbf{v} = \Phi_R^t\lambda \tag{19}$$

$$\Phi_R\Delta\mathbf{v} = \Phi_R\Phi_R^t\lambda \tag{20}$$

The right side of Eq. (20) can be substituted by Eq. (15) as

$$\mathrm{a} = \Phi_R\Phi_R^t\lambda \tag{21}$$

$$\lambda = \left(\Phi_R\Phi_R^t\right)^{-1}\mathbf{a} \tag{22}$$

$$\Phi_R^t\lambda = \Phi_R^t\left(\Phi_R\Phi_R^t\right)^{-1}\mathbf{a} \tag{23}$$

$$\Delta\mathbf{v} = \Phi_R^{-1}\mathbf{a} \tag{24}$$

Finally, the relation between $\delta\mathbf{r}$ and $\Delta\mathbf{v}$ can be written as

$$\Delta\mathbf{v} = \Phi_R^{-1}\delta\mathbf{r} \tag{25}$$

Note, there is no integration, and the state transition matrix is pre-

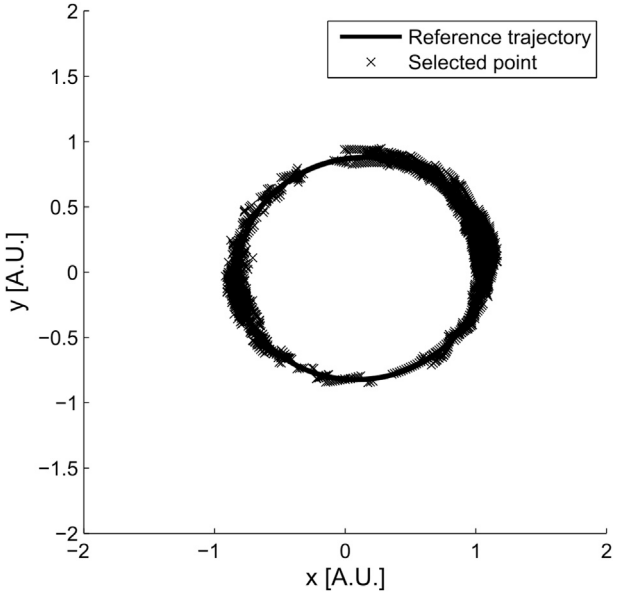

Fig. 5. Third step selection.

computed. The evaluation of this set of equations is very fast, which allowed for 1,137,975 points to be computed in a short time. Once the $\Delta\mathbf{v}$ for each flyby point is calculated, solutions that exceed Eq. (27) (Tsiolkovsky rocket equation) are excluded.

$$\Delta v = \|\Delta\mathbf{v}\| = I_{sp} g_0 \log_e\left(\frac{m_0}{m_f}\right) \tag{26}$$

$$m_f = m_0 - \dot{m}\Delta t_{ToF} \tag{27}$$

where, $g_0 = 9.81$ m/s, $m_0 = 530$ kg and t_{ToF} is time of flight from the beginning of the trajectory up to the flyby date. The resulting selection on step 2 can be seen in Fig. 4, and the number of flyby points after this selection is decreased to 60,283.

Third, and final step, consists in a more sophisticated low-thrust linear approximation [4,6]. Similar to what was done in step 2, the reference trajectory is once again divided into segments. In this case, division is one every half day, with impulses applied in the middle. The objective function to be minimized is a sum of the $\Delta\mathbf{v}$'s, with N being the number of segments,

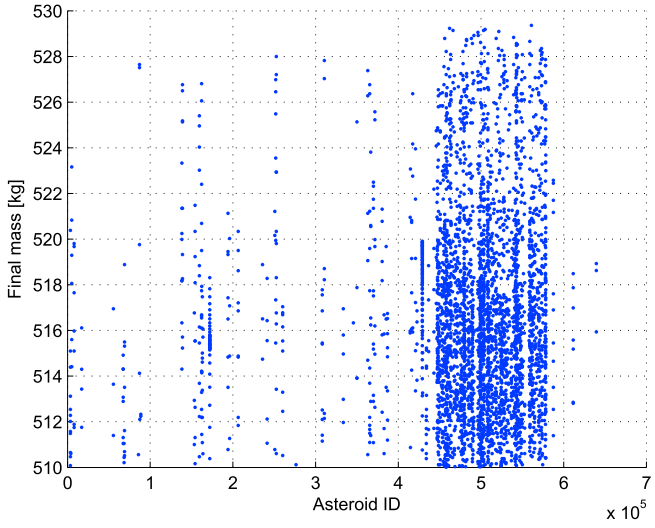

Fig. 6. Linearly estimated final mass for target flyby.

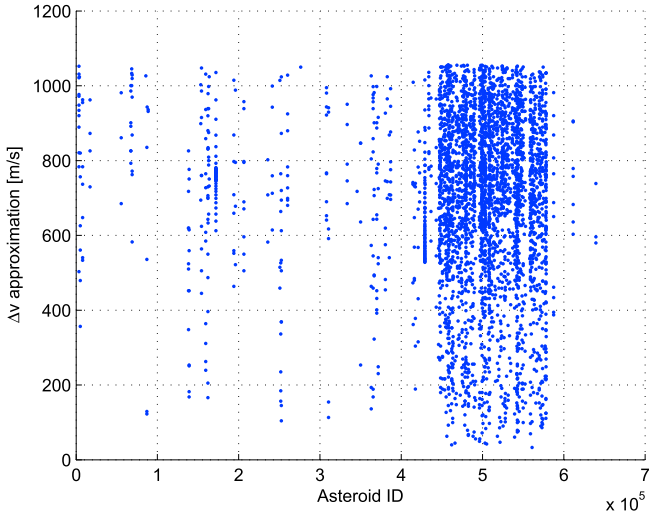

Fig. 7. Linearly estimated Δv for target flyby.

$$J = \sum_{i=1}^{n-1} ||\Delta\mathbf{v}_i|| = \int_{t_0}^{t_f} \|\mathbf{u}(t)\| dt \tag{28}$$

where, $||\mathbf{u}(t)|| = \frac{T(t)}{m(t)} < \frac{T_{max}}{m(t)}$. The thrust law is defined by the sum of the impulses in every segment

$$\mathbf{u}(t)T(t) = \sum_{i=1}^{N} \mathbf{u}_i T_i \mathrm{rect}\left(\frac{t_i}{\Delta t}\right) \tag{29}$$

with $u_i T_i = \alpha_i \Delta\mathbf{v}_i \Delta t$. Where, *rect* is the rectangular function or gate function $rect(x) = 0$ for $|x| > 0.5$ or $= 0.5$ for $|x| = 0.5$ or $= 1$ for $|x| < 0.5$, Δt is the time variation from each node, and $\alpha_i = min(1, \mathbf{u}_{max}\Delta t/|\Delta\mathbf{v}_i|)$. By extension, the state variation due to an impulse is

$$\Delta\mathbf{v}_i = \int_{t_i-\delta t/2}^{t_i+\delta t/2} \mathbf{u}(t)T(t)dt = \mathbf{u}(t)T(t)\Delta t \tag{30}$$

$$\mathrm{x}_{i+1} = \mathrm{x}_i + \begin{bmatrix} \varnothing_{(3\times1)} \\ \alpha_i \Delta\mathbf{v}_i \end{bmatrix} \tag{31}$$

The trajectory is then propagated from t_0 towards t_f until $\alpha = 1$. At this point, all the necessary impulses to reach the target can be given by the

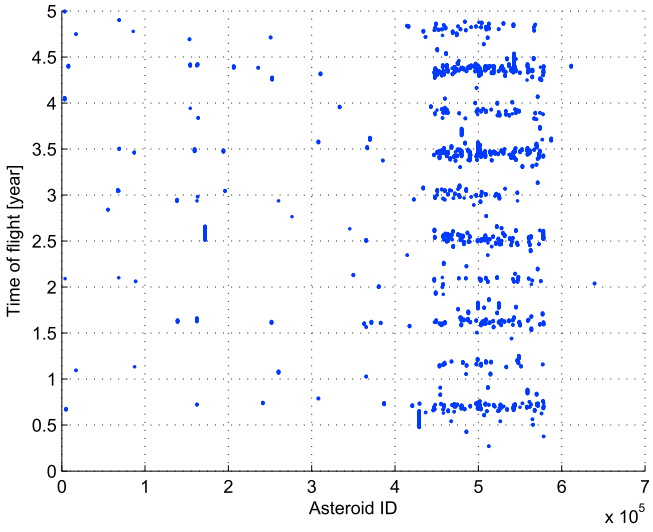

Fig. 8. Linearly estimated ToF for target flyby.

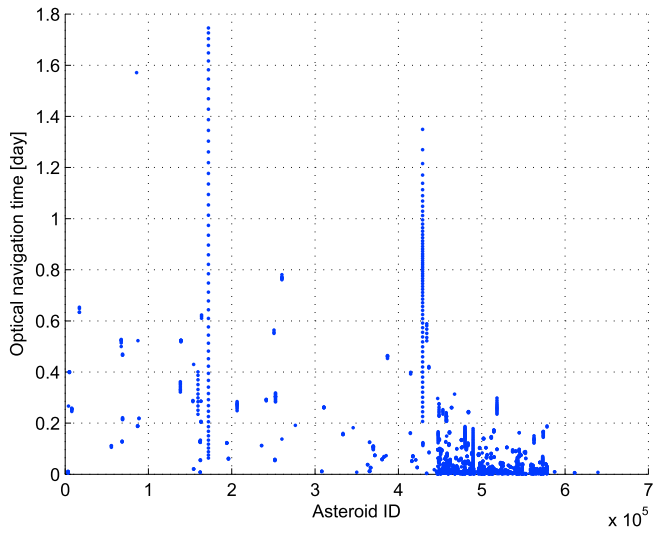

Fig. 9. Linearly estimated optical navigation time for target flyby.

propulsion system. If the propagation finishes and $\alpha = 1$ is not reached, no feasible solution exists. Note, this method also relies on the state transition method, but it loops through the different time steps in order to construct the new trajectory. This loop makes the calculation slower than step 2, but still fast enough to be used with less points. This steps results in 3800 points, Fig. 5, and it also provides an estimation for trajectory states and control profile that can be used in the optimization.

5.2. Target selection results

In total, the search resulted in 3800 flyby points given by 570 asteroid candidates. The main considerations for the select results are: spacecraft final mass and its associated Δv, Figs. 6 and 7 respectively, the time of flight (ToF), Fig. 8, and the optical navigation time, Fig. 9. In the next figures, the x-axis represents the asteroid identification (ID) number according to the database extracted from Ref. [5].

In general, the search was able to identify flyby points on the orbits of a number of asteroids that can be reached with a small ToF, which combined with a small Δv requirement provides many flyby points. Note, asteroids with high ID number generally have several flyby opportunities throughout the 5 years, a fact that is clear by the cluster of points in the plots. Referring to the final mass plot, Fig. 6, asteroids with high ID number also present flyby point with high final mass. Although this targets seem promising at first, the high asteroid ID number represents recent discoveries mainly because they have poor reflectivity and are small. Both are undesirable characteristics for an optical flyby, which is clearly reflected in Fig. 9. An additional issue on newly discovered asteroids is that, in general, their orbits have not been well determined, and there is still a considerable uncertainty in their orbital elements. Therefore, based on the above selection with special regards to the optical navigation time, four target candidates are selected. They can be identified by the four longest optical navigation time solutions in Fig. 9. Table 3 outlines the asteroids' IDs and their two key physical characteristics for optical navigation time calculation: H_{ast} and G_{ast}.

Table 3
Selected target candidates and their physical characteristics.

Asteroid ID	Absolute visual magnitude (H_{ast})	Slope parameter (G_{ast})
(172034) 2001 WR_1	17.9	0.15
(85713) 1998 SS_{49}	15.6	0.15
(429094) 2009 SG_2	20.1	0.15
(260141) 2004 QT_{24}	18.3	0.15

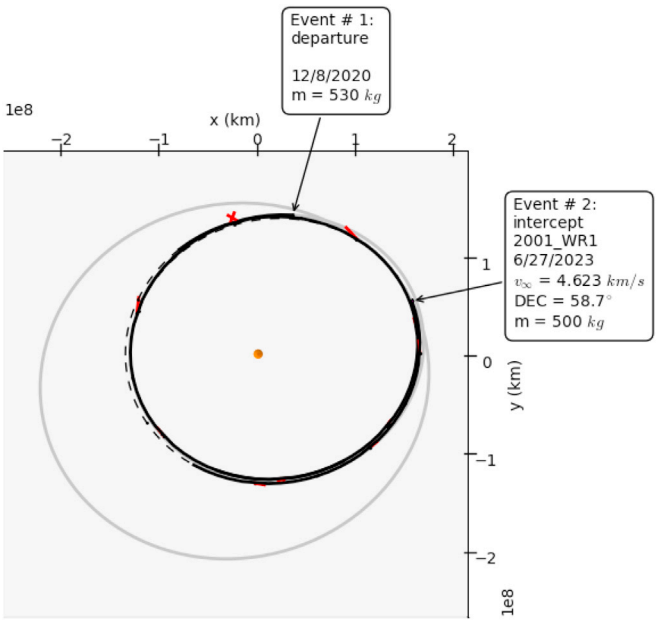

Fig. 10. Trajectory design for (172034) 2001 WR_1.

6. Trajectory design

Once the target selection is done, the candidates are considered in the non-linear low-thrust trajectory optimization. The objective function continues to be the maximization of the optical navigation time, given the fuel and propulsion constraints. In the optimization process, the target candidates are added as flyby constraints to the problem with a flight time of less than or equal to five years. An initial estimation for the optimization states and control are obtained in the last step of the selection process.

The trajectory optimization is then performed by the Evolutionary Mission Trajectory Generator (EMTG). EMTG is NASA Goddard's fully automated tool for the design of interplanetary missions using either high-thrust chemical or low-thrust electric propulsion as well as planetary flyby maneuvers. It is capable of determining both the optimal flyby sequence and spacecraft systems configuration (using an integer genetic algorithm) as well as the optimal trajectory (using a nonlinear programming solver and monotonic basin hopping). The tool models a wide variety of operational constraints and includes medium-fidelity models of launch vehicle, thruster, and power system performance. EMTG is distributed open-source [14]. The monotonic basin hopping [15] is of special interest for this problem, because it allows the optimization tool to “hop” from one local minimum to the next one, increasing the likelihood of finding the global minimum. This is a very desirable characteristic for solving problems that can span a long time and generate several local minima. Without this feature, the solution would simply converge to the closest basin with the risk of having a better solution, a larger optical navigation time, at another date.

The simulations also include third body perturbation from Earth using a finite burn low-thrust model [15]. This is an important addition to correctly account for the states direction after the Earth escape. Although Hayabusa 2 has a fast Earth escape, the planet still influences the spacecraft's trajectory during the initial days when the vehicle lies inside Earth's sphere of influence.

The low-thrust trajectories that maximize the optical navigation time for the four target candidates selected on the previous section can be seen in Figs. 10–13. These are in the same order as presented in Table 3.

The following Table 4 summarizes the most important trajectory characteristics for this extension proposal.

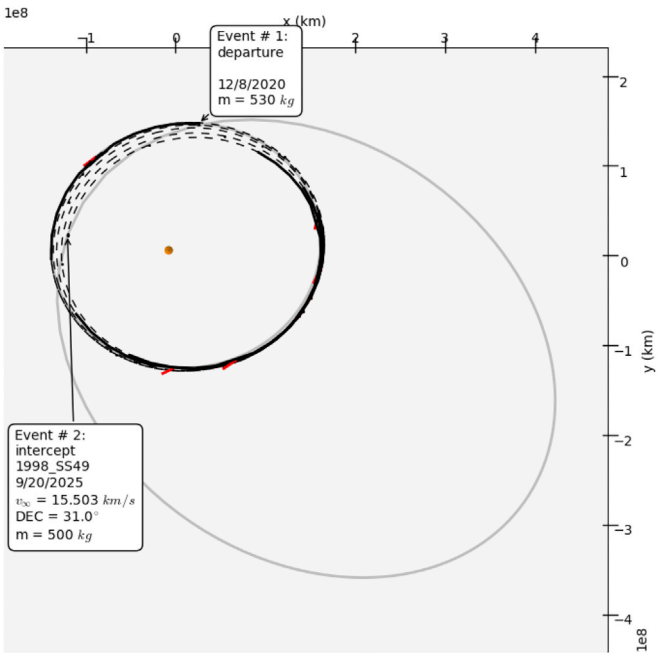

Fig. 11. Trajectory design for (85713) 1998 SS_{49}.

Here, the best solution found is considered for the asteroid (172034) 2001 WR_1, which has the biggest optical navigation time and shortest ToF. Both factors contribute to the mission robustness. The large optical navigation time is due to the combination of the asteroid's absolute visual magnitude, the spacecraft's small v_∞ and solar phase angle at arrival. The first allows time for the target identification and TCM, and the second for reliability on the subsystems.

7. Conclusions

This work is dedicated to the target selection and trajectory design proposal for the Hayabusa 2 mission extension. Hayabusa 2 nominal mission objective is to study the asteroid Ryugu, (162173) 1999 JU_3, and return surface and subsurface samples to Earth for further analysis. The extension proposal starts from a fixed initial escape condition from Earth after the sample capsule is released. In it, this study considered the spacecraft conditions at the final Earth encounter, as well as an extensive database for possible target candidates. System level requirements were taken into account in the target selection and trajectory design.

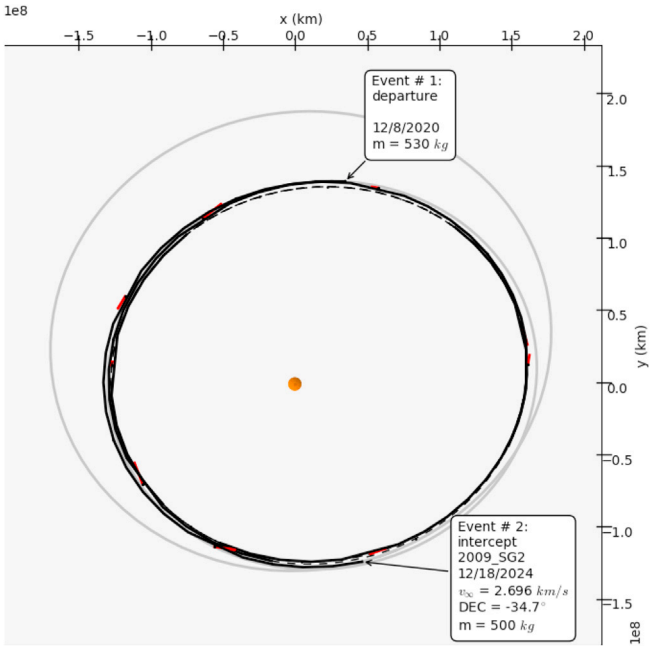

Fig. 12. Trajectory design for (429094) 2009 SG_2.

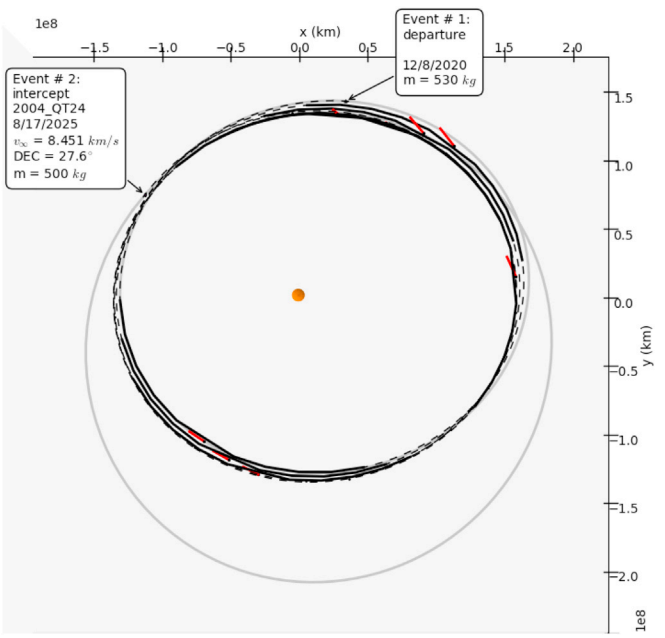

Fig. 13. Trajectory design for (260141) 2004 QT_{24}.

Table 4
Trajectory optimization results.

Asteroid ID	Final mass [kg]	ToF [day]	Opt. nav. [day]	v_∞ [km/s]	SPV [degree]
(172034) 2001 WR_1	500	932	1.568	4.62	48.77
(85713) 1998 SS_{49}	500	1748	0.457	15.50	117.80
(429094) 2009 SG_2	500	1417	1.050	2.70	58.40
(260141) 2004 QT_{24}	500	1714	0.204	8.45	108.40

The target selection resulted in four possible targets from a database of over 700,000 asteroid candidates, with the final low-thrust trajectory optimization considers Earth third body perturbation and spacecraft operational constraints. The main mission extension requirement was to provide the spacecraft enough optical navigation time at target arrival for identification and trajectory correction maneuvers. With this, the trajectory results of the four selected targets were assessed in three key points: final mass, time of flight and optical navigation time. Based on this study, the asteroid (172034) 2001 WR_1. is proposed as the Hayabusa 2 mission extension target with a flyby on 27 of June 2023. The resulting trajectory used all the available xenon with 100% duty cycle finishing with 500 kg, lasting for 932 days and reaching 1.581 days of optical navigation time.

References

[1] J. Kawaguchi, A. Fujiwara, T. Uesugi, Hayabusa - its technology and science accomplishment summary and Hayabusa-2, Acta Astronaut. 62 (10–11) (May-June 2008) 639–647, http://dx.doi.org/10.1016/j.actaastro.2008.01.028.
[2] Y. Tsuda, M. Yoshikawa, M. Abe, H. Minamimo, S. Nakazawa, System design of the Hayabusa 2-asteroid sample return mission to 1999 JU3, Acta Astronaut. 91 (October-November 2013) 356–362, http://dx.doi.org/10.1016/j.actaastro.2013.06.028.

[3] N.A. Moskovitz, et al., Rotational characterization of Hayabusa II target asteroid (162173) 1999 JU3, Icarus 224 (1) (May 2013) 24–31, http://dx.doi.org/10.1016/j.icarus.2013.02.009.
[4] B.V. Sarli, Y. Kawakatsu, Selection and Trajectory Design to Mission Secondary Targets, Celestial Mechanics and Dynamical Astronomy, 2016 (Accepted).
[5] Minor Planet Center, The MPC Orbit Database. http://www.minorplanetcenter.net/iau/MPCORB.html (Accessed 28 October 2015).
[6] B.V. Sarli, C. Yam, Y. Kawakatsu, Low-thrust trajectory design for the DESTINY Mission to (3200) phaethon, in: AAS 16-387, 26th AAS/AIAA Space Flight Mechanics Meeting, Napa, CA, February 14-18, 2016.
[7] J. Englander, B. Conway, T. Williams, Automated solution of the low-thrust interplanetary trajectory problem, J. Guid. Control, Dyn. 40 (1) (2017) 15–27, http://dx.doi.org/10.2514/1.G002124.
[8] J. Englander, M. Vavrina, Global optimization of low-thrust interplanetary trajectories subject to operational constraints, in: AAS 16-239, 26th AAS/AIAA Space Flight Mechanics Meeting, Napa, CA, February 14-18, 2016.
[9] O.R. Norton, The Cambridge Encyclopedia of Meteorites, Cambridge University Press, Cambridge, 2002, p. 121124. ISBN 0-521-62143-7.
[10] S.M. Lederer, et al., Physical characteristics of Hayabusa target asteroid 25143 Itokawa, Icarus 173 (2005) 153165, http://dx.doi.org/10.1016/j.icarus.2004.07.022.
[11] Japan Aerospace Exploration Agency, Asteroid Explorer "Hayabusa2". http://global.jaxa.jp/projects/sat/hayabusa2/ (Accessed 23 August 2016).
[12] B.V. Sarli, G. Rivier, Y. Kawakatsu, Design of a proximity flyby trajectory using optimal control theory and genetic algorithm, in: IAC-14–C1.7.6, 65th International Astronautical Congress, Toronto, Canada, September 29-October 3, 2014.
[13] R. Dymock, The H and G Magnitude System for Asteroids, The BAA Observers' Workshops, Milton Keynes, February, 2007.
[14] J.A. Englander, B.A. Conway, An automated solution of the low-thrust interplanetary trajectory problem, J. Guid. Control, Dyn. AIAA 40 (1) (2017) 15–27, http://dx.doi.org/10.2514/1.G002124.
[15] J.A. Englander, A.C. Englander, Tuning monotonic Basin hopping: improving the efficiency of stochastic search as applied to low-thrust trajectory optimization, in: 24th International Symposium on Space Flight Dynamics, ISSFD, Laurel, MD, May, 2014.